

DEPTH PROFILE RECONSTRUCTION FROM RUTHERFORD BACKSCATTERING DATA

U. V. TOUSSAINT, K. KRIEGER, R. FISCHER, V. DOSE
Max-Planck-Institut für Plasmaphysik, EURATOM Association
POB 1533, D-85740 Garching, Germany[†]

Abstract. An adaptive kernel method in the Bayesian framework together with a new simulation program for Rutherford backscattering spectroscopy (RBS) have been applied to the analysis of RBS data. Even in the case of strongly overlapping RBS peaks a depth profile reconstruction without noise fitting has been achieved. The adaptive kernel method leads to the simplest depth profile consistent with the data. Erosion and redeposition rates of carbon divertor plates in the fusion experiment ASDEX Upgrade could be determined by RBS-analysis of thin film probes before and after exposition to plasma discharges.

Key words: Rutherford Backscattering, Inverse Problem, Deconvolution

1. Introduction

Rutherford backscattering is one of the most important and most commonly applied techniques in surface analysis. Its main advantages are that it is fully quantitative and that precisions less than 1% can be achieved [1]. The interpretation of the data, however, is in many cases not straightforward. During the last decade several computer programs for the simulation and analysis of spectra obtained from RBS were developed, such as RUMP [2] or SIMNRA [3]. With these programs the determination of a depth profile is, however, a matter of trial and error. The user has to prescribe depth profiles of all elements and has to compare the simulated spectrum calculated from the input profiles with the data. The depth profiles are then adjusted until one obtains a reasonable agreement of simulated and measured data. Obviously this evaluation procedure has several shortcomings. It is a time-consuming cumbersome task, the accuracy of the achieved depth profile is unknown and in many cases there is an ambiguity between different depth profiles which fit the data equally well. The combination of the adaptive kernel method in the Bayesian framework [4] with an RBS-simulation program allows to overcome these disadvantages and extends the potential of Rutherford backscattering spectroscopy.

[†]Email: udo.v.toussaint@ipp.mpg.de

2. Basic Concepts of Rutherford Backscattering

In RBS-analysis, a sample is exposed to a beam of ions with mass m_0 (e.g. He-particles) with a well defined energy E_0 in the order of MeV. Ions undergoing elastic Coulomb collisions with sample atoms are recorded in a solid state detector which views at a fixed deflection angle θ . The Rutherford cross-section for this coulombic projectile-target interaction is quantitatively known. The energy E' of the backscattered ions depends on the energy E before the collision, the mass of the ions m_0 , the mass of their colliding partner M_i and the deflection angle θ :

$$E' = E \left[\frac{\sqrt{1 - \left(\frac{m_0}{M_i}\right)^2 \sin^2 \theta} + \frac{m_0}{M_i} \cos \theta}{1 + \frac{m_0}{M_i}} \right]^2. \quad (1)$$

From Eq. 1 we see that ions undergoing a collision with a heavy target atom loose less energy than ions colliding with a target atom of lower atomic mass. In addition, both primary ions and scattered ions loose energy on their way through the sample, depending on the stopping power. This is the main reason which enables RBS to be depth sensitive. The stopping power depends on the energy of the particles and the composition of the sample.

Fig. 1a depicts a typical RBS experiment. A thin overlayer (A) of atoms with a

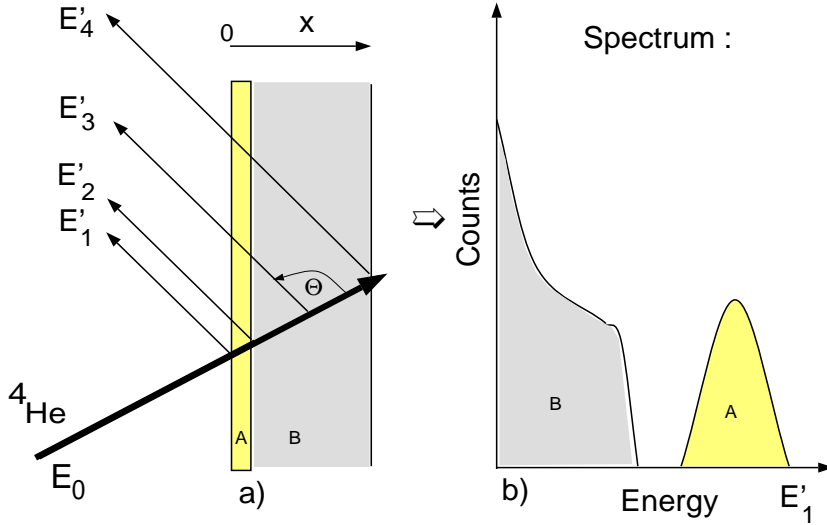


Figure 1. Schematic diagram of a RBS-experiment a) and the corresponding spectrum b).

high atomic mass M_A is on top of the bulk substrate (B) with a lower atomic mass M_B . In the energy spectrum of backscattered particles (Fig. 1b), the film A leads to a spectral peak at higher energies, broadened by the apparatus transfer function and the statistical fluctuations of the energy loss of the ions. Scattering

from B produces a broadened step at lower energies. The high energy side of this step originates from scattering from the topmost B-Layer. The increase of the spectrum with decreasing energy results mainly from the $\frac{1}{E^2}$ dependence of the Rutherford cross section.

3. Simulation of RBS-Spectra

For a spectrum synthesis the sample is divided into sub-layers with thickness Δx . The spectrum is calculated from the superimposed contributions of scattering processes from all elements in all sub-layers of the sample. For each sub-layer the concentrations on the layer-boundaries must be given. Inside the sub-layer the concentration profile is assumed to interpolate linearly. In each sub-layer the energy loss of the ions inside this layer and the cross-sections are determined.

Cross-Section Data: The actual cross-section deviates from the well known Rutherford cross-section [5] at both, high and low energies. The low-energy discrepancy is caused by partial screening of the nuclear charges by the electronic shells [5]. This screening is taken into account by a correction factor $C(E, \Theta)$ [6]. At high energies the cross sections deviate from the Rutherford cross-section due to the influence of the nuclear force [7]. This is unimportant in the present case.

Stopping Power Data: The two dominant processes of energy loss of a penetrating ion are the interactions of the moving ion with bound or free electrons in the target, and the interactions of the moving ion with the screened or unscreened nuclei of the target atoms. The electronic stopping power data are taken from Ziegler, Biersack and Littmark [8]. The nuclear stopping power for helium is calculated from [8]. In compound materials, Bragg's rule is used,

$$\left(\frac{dE}{dx}\right)_{total} = \sum_i c_i \left(\frac{dE}{dx}\right)_i, \quad (2)$$

to calculate the effective stopping power $\left(\frac{dE}{dx}\right)_{total}$ from the concentrations c_i and the stopping power $\left(\frac{dE}{dx}\right)_i$ of each individual component i . The key assumption of Bragg's rule that the interaction between the ion and a target atom is independent of the environment holds in most cases. In some compounds such as oxides the deviations from Bragg's rule predictions may, however, be of the order of 10% to 20% [9].

Energy Loss Straggling: The energy loss of charged particles penetrating material is accompanied by a spread of the beam energy which is due to statistical fluctuations of the energy transfer in the loss channels. As the number of interactions is high, the energy broadening is well described by a Gaussian. The program uses Bohr's theory of energy-loss straggling [10], together with corrections by Chu [11], which include the electron binding in the target atoms. The energy dependence of the stopping power results further in a non-stochastic broadening (or squeezing)

of the energy distribution of the ion beam. The energy width ΔE_f after passing the sub-layer is given by [12]:

$$\Delta E_f = \frac{S(E_f)}{S(E_i)} \Delta E_i \quad (3)$$

with E_i , E_f as the mean energies and $S(E_i)$, $S(E_f)$ as the stopping powers at the entrance and exit of the sub-layer, respectively.

4. Experiment

The interpretation of RBS data is required for the analysis of erosion measurements of plasma facing materials in fusion experiments. The solid inner walls surrounding the plasma are subjected to an intense bombardment by plasma particles because the confinement of the plasma by the confining magnetic field is not perfect. The surfaces of the inner walls are mainly modified by ion implantation, erosion and by deposition of material from other wall areas.

One major problem in fusion research is to find a wall material where wall erosion rate and wall modifications are small and tolerable [13]. The importance of this problem for planned fusion power plants is emphasized by an erosion analysis for ITER [14]. The modeled gross erosion yield of a carbon-divertor could reach a maximum of 5m/burning-year, which is reduced by redeposition down to about 0.5m/burning-year. The modeling, however, faces exceptional difficulties due to complex hydrocarbon transport phenomena and the lack of input data (e.g. for low energy sputtering). Therefore experimental determination of erosion and redeposition yields is necessary to validate the modeling and to improve the quantitative knowledge of the fundamental erosion processes.

To determine carbon erosion rates in the divertor of ASDEX Upgrade, graphite probes which were covered with a 150nm layer of ^{13}C were exposed to single plasma discharges. ^{13}C was used because chemical erosion is unaffected by isotope substitution and to allow the measurement of redeposited ^{12}C eroded at other plasma facing components. Furthermore the stopping power in ^{13}C and ^{12}C is the same and so the limited accuracy of the stopping power in the simulation cancels. The sample was introduced in the outer divertor of ASDEX Upgrade (circle in Fig. 2) covering in particular the strike point, which is the point where the outermost last closed magnetic flux line touches the plate surface with a corresponding maximum of the power load.

The samples were analyzed before and after plasma exposure with a total exposure time of 4 seconds using RBS with 2.0 MeV ^4He ions. The backscattered particles were detected at a scattering angle of $\Theta = 165^\circ$. The width of the apparatus transfer function is about 19keV FWHM [15]. Fig. 3 shows typical spectra before and after plasma exposure. Before plasma exposure the signal from the ^{13}C -layer at higher energy is separated by a gap from the part of the spectrum corresponding to the underlying ^{12}C -bulk material. After plasma exposure the high energy edge of the signal from ^{13}C has shifted towards lower energies. This indicates that there is no longer ^{13}C at the surface of the sample. The peak at 430 keV is due to the ^{12}C at the sample surface and from the ^{13}C fraction below the surface. The difference

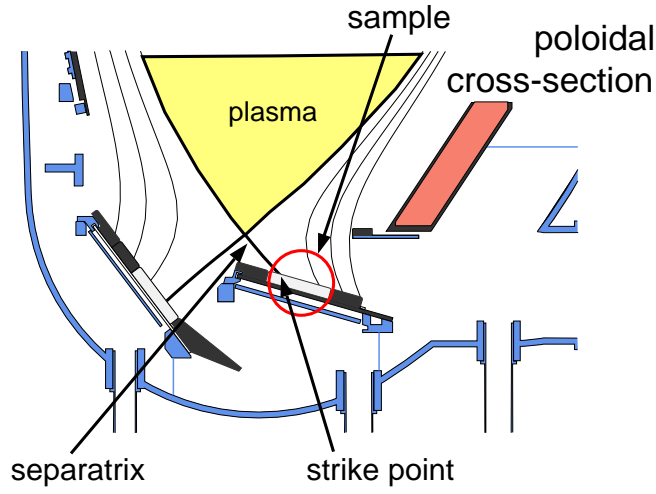


Figure 2. Poloidal cross-section of ASDEX-Upgrade. The circle indicates the position of the sample on the outer divertor in ASDEX-Upgrade. The separatrix is the outermost closed magnetic flux line. The point the separatrix touches the divertor is called the strike point

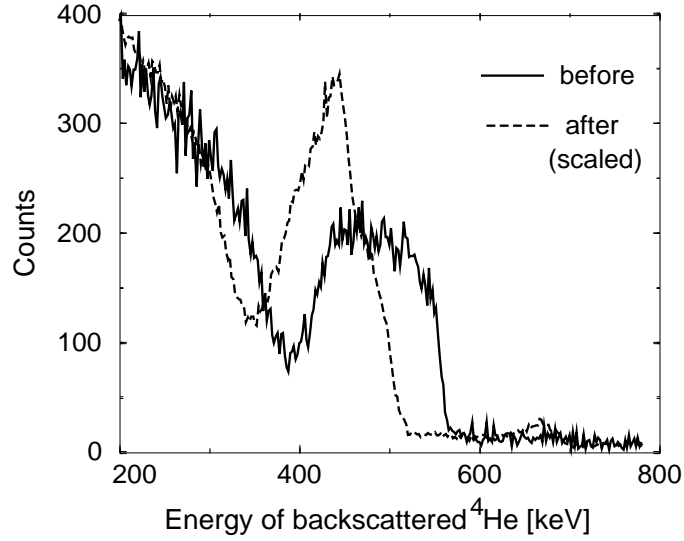


Figure 3. RBS-spectra before and after plasma exposure. The shift of the high energy edge is clearly visible.

of the RBS-spectra before and after exposure contains the information about the erosion and redeposition yields.

5. Results

To determine the concentration depth profiles from the measured RBS data a simple χ^2 -fit is insufficient and results in useless rapidly oscillating depth profiles. This is due to the ill-conditioned nature of the inversion problem which results from the energy-straggling broadening, the finite apparatus-induced energy resolution and the counting statistics. Furthermore the optimal grid, given by the thickness of the sub-layers the sample is divided in, is unknown.

For this kind of problems the adaptive kernel method is well suited. The concept of adaptive kernels provides local smoothness which makes the result robust against noise corruption. The locality of the information content of the data is taken into consideration by the local varying kernel widths. Constraints like positivity or other prior knowledge (like bulk concentrations) are easy to include. The used adaptive kernel method is presented in detail in this proceeding [16].

Fig. 4a shows the reconstructed ^{12}C and ^{13}C -depth profiles of a sample before

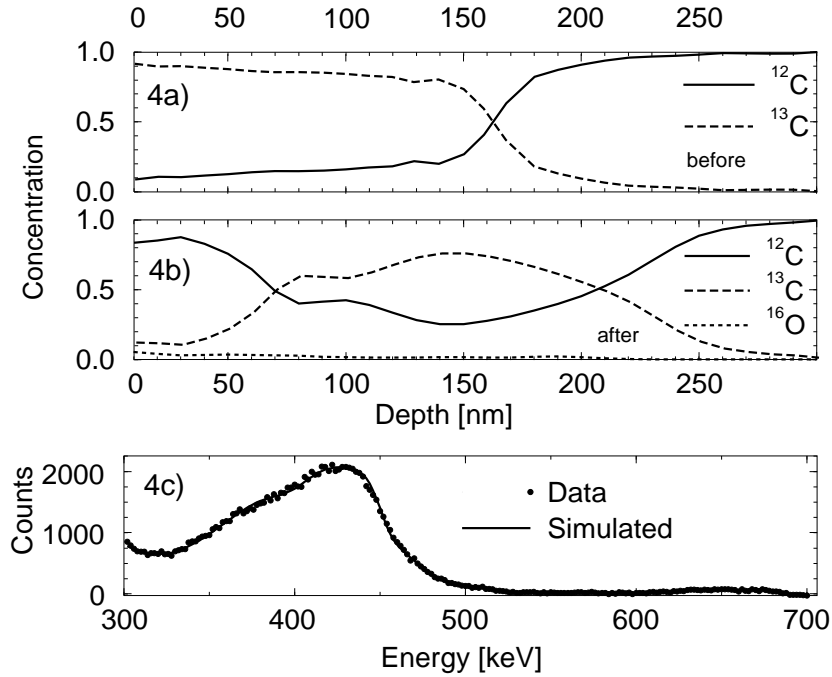


Figure 4. panels a) and b): ^{12}C and ^{13}C -distribution before and after plasma exposure. Panel c): RBS-data (black dots) and the calculated RBS-spectrum (grey line) from the depth profile in the panel b).

plasma exposure. The concentrations in each layer sum up to one. The surface concentration of ^{13}C (on the left side) is above 90% and decreases only slightly to a depth of about 150nm. The remaining 10% fraction of ^{12}C is caused by impurities in the coating process. The broad transition between the ^{13}C -layer and the ^{12}C -bulk can be explained by the interface roughness of the virgin sample.

After 4 seconds of plasma exposure the depth profiles have changed dramatically, as shown in Fig. 4b. There is a ^{12}C -layer with a thickness of about 70nm on top of the ^{13}C . The maximum concentration of ^{13}C has decreased, however, the thickness of the ^{13}C -layer is with about 170nm nearly unchanged. Furthermore, there is a continuous level of ^{12}C in the whole sample with a minimum concentration of 20%. Since diffusion due to thermal effects could be excluded, the impacting ^{12}C -atoms must have mixed the material. Fig. 4c shows the RBS-data as black dots and the calculated RBS-spectrum (solid line) based on the depth profile shown in Fig. 4b. The agreement is within the counting statistics.

With samples in different distances to the strike point we achieved a laterally resolved determination of erosion and deposition as shown in Fig. 5. The height of the ^{13}C -tracer was 153nm before exposure (dashed line in Fig. 5). The grey shaded

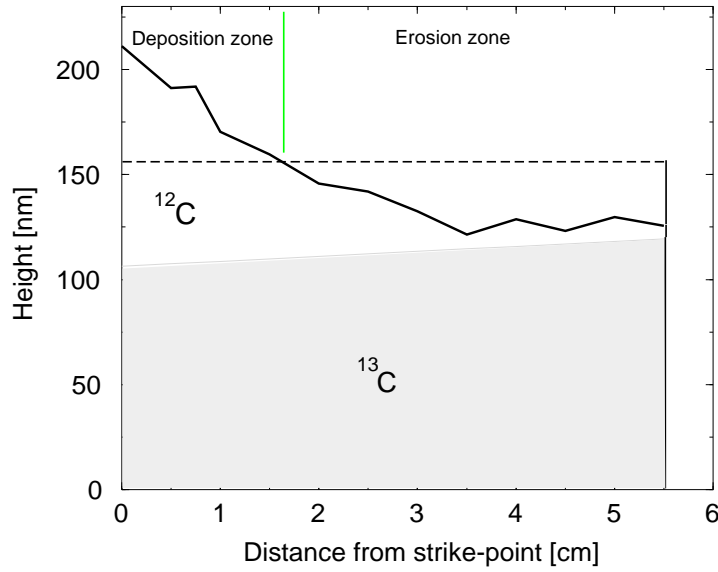


Figure 5. Schematic picture of the ^{12}C and ^{13}C distribution before and after plasma exposure. The grey dashed line gives the height of the ^{13}C -tracer before plasma exposure. The grey shaded area marks the height of ^{13}C after plasma exposure and the difference between the upper black line and the grey shaded area gives the height of deposited ^{12}C .

area marks the thickness of the ^{13}C -layer after plasma exposure. The highest erosion of 40nm was observed at the strike point. With increasing distance the erosion reduces slightly to $\approx 30\text{nm}$ in 5cm distance. The solid line represents the joint height of the ^{13}C and deposited ^{12}C under the assumption that no ^{12}C from the bulk was eroded. The difference between the solid line and the grey shaded area of ^{13}C is the height of deposited ^{12}C . The amount of ^{12}C which covers the ^{13}C is largest at the strike point with over 100nm and reduces down to 10nm in a distance of 5.5cm. Near the strike point the redeposition of carbon is larger than the erosion, which makes this location a net deposition zone. By contrast, in a distance larger than 1.5cm from the strike point there is a net erosion area.

Fig. 5 is only a schematic representation which shows the total amount of ^{12}C and ^{13}C in a simplified distribution. It can be seen from the depth profiles in Fig. 4 that after plasma exposure there are no longer clearly separated layers of the two different isotopes and pronounced mixing has occurred. The large spatial variation of erosion and deposition rates shows, that the lifetime of plasma facing components can only be evaluated for specific local conditions.

6. Conclusions

With the used combination of the RBS-simulation program and the adaptive kernel method the capabilities of RBS-data evaluation have been considerably extended. This allows to study erosion, deposition and mixing of carbon as inner wall material in fusion experiments by using different isotopes which have no influence on the chemical erosion. The experiment shows a spatially varying net erosion/deposition rate with large mixing. Further investigations are necessary to answer the question of the long-time behavior of the erosion of the inner wall materials facing different plasma conditions.

References

1. C. Jeynes, Z. H. Jafri, R. P. Webb, A. C. Kimber, and M. Ashwin *Surface and Interface Analysis*, **25**, p. 254, 1997.
2. L. R. Doolittle *Nucl. Instr. and Meth. B*, **9**, p. 291, 1985.
3. M. Mayer, "Simnra user's guide," *Max-Planck-Institut für Plasmaphysik, Technical Report*, **9**, p. 113, 1997.
4. R. Fischer, M. Mayer, W. von der Linden, and V. Dose *Phys. Rev. E*, **55**, p. 6667, 1997.
5. J. Tesmer and M. Nastasi, eds., *Handbook of Modern Ion Beam Materials Analysis*, Materials Research Society, Pittsburgh, Pennsylvania, 1995.
6. H. Anderson, F. Besenbacher, P. Loftager, and W. Moeller *Phys. Rev. A*, **21**, p. 1891, 1980.
7. M. Bozoin in *Handbook of Modern Ion Beam Materials Analysis*, J. Tesmer and M. Nastasi, eds., Materials Research Society, Pittsburgh, Pennsylvania, 1995.
8. J. Ziegler, J. Biersack, and U. Littmark, *The Stopping and Ranges of Ions in Matter*, vol. 1, Pergamon Press, New York, 1985.
9. J. Ziegler and J. Manoyan *Nucl. Instr. Meth. B*, **35**, p. 215, 1988.
10. N. Bohr *Mat. Fys. Medd. Dan. Vid. Selsk.*, **18**, 1948.
11. W. Chu *Phys. Rev.*, **13**, p. 2057, 1976.
12. E. Szilagy, F. Pászti, and G. Amsel *Nucl. Instr. Meth. B*, **100**, p. 103, 1995.
13. R. Behrisch *Phys. Res.*, **8**, p. 569, 1988.
14. J. N. Brooks, D. Alman, G. Federici, D. N. Ruzic, and D. G. White, "Erosion/redeposition analysis: status of modeling and code validation for semi-detached edge plasmas," in *13th International Conference on Plasma Surface Interactions in Controlled Fusion Devices*, San Diego, California, 1998.
15. V. Dose, R. Fischer, and W. von der Linden, "Deconvolution based on experimentally determined apparatus functions," in *Maximum Entropy and Bayesian Methods*, J. Rychert, G. Erickson, and R. Smith, eds., Kluwer Academic Publishers, Dordrecht, 1998.
16. R. Fischer, W. Jacob, W. von der Linden, and V. Dose, "Bayesian reconstruction of electron energy distributions in helium plasmas from emission line intensities," in *Maximum Entropy and Bayesian Methods*, V. Dose, W. von der Linden, R. Fischer, and R. Preuss, eds., Kluwer Academic Publishers, Dordrecht, 1999.